Hexaazatriphenylene-Based, Hydrogen-Bonded Organic Framework with Permanent Porosity and Single-Crystallinity: Synthesis, Structural, Uptaking and Photophysical Characterization

Ichiro Hisaki,*[a] Nobuaki Ikenaka,[a] Eduardo Gomez,[b] Boiko Cohen,[b] Norimitsu Tohnai,[a] and Abderrazzak Douhal*[b]

Abstract: Hydrogen-bonded organic frameworks (HOFs) have drawn unprecedented interests because of their high crystallinity as well as facile process for construction, deconstruction, and reassembly arising from reversible bond formation-dissociation. However, structural fragility and low stability frequently prevent formation of robust HOFs with permanent porosity. Herein, we report that hexakis(4-carboxyphenyl)-hexaazatriphenylene (**CPHAT**) forms three dimensionally networked H-bonded framework **CPHAT-1**. Interestingly, the activated framework **CPHAT-1a** retains not only permanent porosity but single-crystallinity, enabling precise structural characterization and property evaluation on a single crystal. Moreover, **CPHAT-1a** retains its framework up to 339 °C or in hot water and in acidic aqueous solution. These results clearly show that even a simple H-bonding motif can be applied for construction of robust HOFs, which creates a pathway to establish a new class of porous organic frameworks. We also characterize its uptake of gases and I_2, in addition to a detailed photophysical study (spectroscopy and dynamics of proton and charge transfers) of its unit in solution, and of its single crystal under fluorescence microscopy, where we observed a marked strong anistropy and narrow distribution. The results bring new findings to advance in HOFs and their possible applications in science and technology.

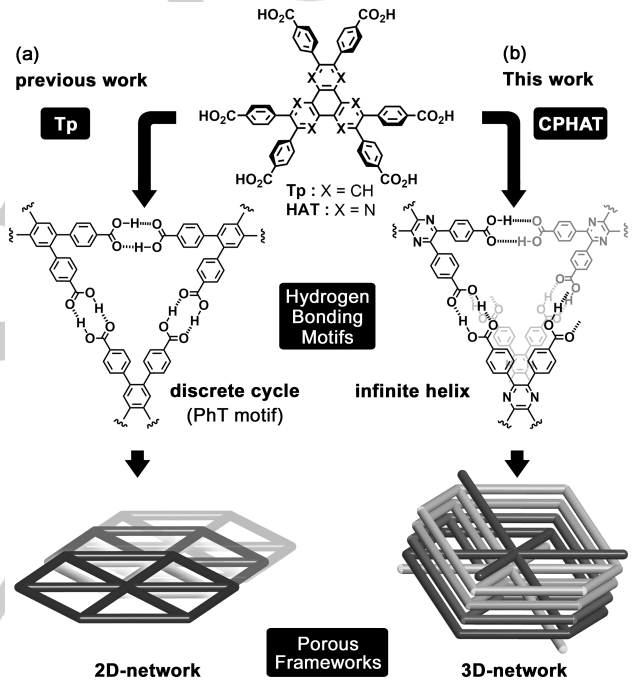

Figure 1. Formation of Hexagonally Networked porous frameworks based on C_3-symmetric π-conjugated molecules possessing six carboxyphenyl groups in periphery. (a) **Tp** yields layered assembly of 2D-network through discrete cyclic hydrogen bonding motif so-called PhT as reported previously. (b) **HAT** yields 4-fold interpenetrated 3D-network through infinite helical hydrogen bonding motif.

Introduction

Porous frameworks constructed by organic molecules are currently one of the central interests in the fields of materials chemistry and crystal engineering.[1] Particularly, networking through reversible hydrogen-bonds (H-bonds) frequently provides frameworks with high crystallinity due to self-repairing of irregular molecular connection, allowing precise structural analysis and insight of structure-property relationships. Meanwhile, relatively weak bonding strength of H-bonds cases fragility of frameworks and lack of universalistic design principles. To overcome this problem, various supramolecular synthons[2] have been applied, resulting in fascinating H-bonded organic frameworks (HOFs)[3] with permanent porosity.[4]

A dimer of carboxyl groups, which is one of the simplest and commonest supramolecular synthon,[2,5] is also appropriate to construct HOFs due to significantly directional nature and facile synthesis of derivatives.[6] For example, Zentner et al. reported a porous framework composed of interpenetrated honeycomb sheets of 1,3,5-tris(4-carboxyphenyl)benzene.[7a] Vaidhyanathan reported tripodal tricarboxylic acid molecule with flexible sp^3

[a] Dr. I. Hisaki, N. Ikenaka, Dr. N. Tohnai
Department of Material and Life Science, Graduate School of Engineering, Osaka University, 2-1 Yamadaoka, Suita, Osaka 565-0871 (Japan)
E-mail: hisaki@mls.eng.osaka-u.ac.jp
[b] *E. Gomez, Dr. B. Cohen, Prof. Dr. A. Douhal*
Departamento de Quimica Fisica, Facultad de Ciencias Ambientales y Bioquimica, and INAMOL, Universidad de Castilla-La Mancha, Avenida Carlos III, S/N, 45071 Toledo (Spain)
Abderrazzak.Douhal@uclm.es

Supporting information for this article is given via a link at the end of the document.

nitrogen center yields HOFs exhibiting selective CO_2 sorption behavior.[7b] More recently, Wu and Yuan et al. demonstrated that a significantly stable HOF with high surface area was nicely formed with 3,3',5,5'-tetrakis-(4-carboxyphenyl)-1,1'-biphenyl.[7c] However, examples of the carboxyl dimer-based HOFs with permanent porosity and high crystallinity are still limited.

In connection with this, we also reported that C_3-symmetric planar π-conjugated hydrocarbons, such as triphenylene (**Tp**), possessing three 4,4'-dicarboxy-*o*-terphenyl moieties in periphery form porous hexagonal network (HexNet) structures through the cyclic H-bonded motif so-called phenylene triangle (PhT), and that the HexNet sheet stacks without interpenetration to give flexible layered HOFs with permanent porosity (Figure 1a).[8] In the present work, we used a heterocyclic π-conjugated system, hexaazatriphenylene (HAT)[9] with six carboxyphenyl groups, as a building block and achieved a significantly rigid HOF **CPHAT-1** (Figure 1b). HAT has been investigated as electron and/or hole transport materials in organic semiconducting devices,[9] mesogens of liquid crystals,[9] ligands of metal complexes,[10] building blocks of porous materials such as metal organic frameworks (MOFs)[11] and covalent organic frameworks (COFs)[12] due to its rigid, planar, π-conjugated skeleton with nitrogen atoms. However, this is the first example of HAT-based HOF with permanent porosity. The derivatives with six carboxyphenyl groups in periphery (**CPHAT**) yields three-dimensionally networked rigid ***pcu***-framework with permanent porosity, instead of 2D layered ***hxl***-framework as in the case of **Tp**.[8]

One of the most significant nature of the present system is that the activated framework **CPHAT-1a** retains not only permanent porosity, but single-crystallinity after activation. Furthermore, the framework is thermally stable up to 339 °C and has resistance against hot water and even aqueous hydrochloric acid. Such robust framework built by carboxylic acid dimer is hitherto unknown.

Herein, we present synthesis of **CPHAT**, preparation of rigid HOF **CPHAT-1**, its thermal behaviours, gases and iodine sorption properties of the activated HOF **CPHAT-1a**, and detailed photophysical behaviour in solutions, crystalline bulks, and single crystals. For the latter, we observed a remarkable fluorescence anisotropy behaviour reflecting the molecular alignment of the units within the crystal.

Results and Discussion

Synthesis and crystallization.

Hexaaminobenzene (**2**) was synthesized by hydration of 1,3,5-triamino-2,4,6-trinitrobenzene (**1**) according to the literature.[13] Triple condensation of **2** with dione **3** in acidic condition yielded hexaazatriphenylene derivative **4** in 83% yield in two steps from **1**. Hydrolysis of **4** gave **CPHAT** in 93%. **CPHAT** was recrystallized by slow evaporation from a mixed solution of *N*,*N*-dimethylformamide (DMF) and 1,2,4-trichlorobenzene (TCB). At 100 °C, **CPHAT** yielded a solvated HOF crystal **CPHAT-1-(TCB)**, in which all carboxylic groups of **CPHAT** formed H-bonding dimer to give a networked porous framework (*vide infra*). At relatively

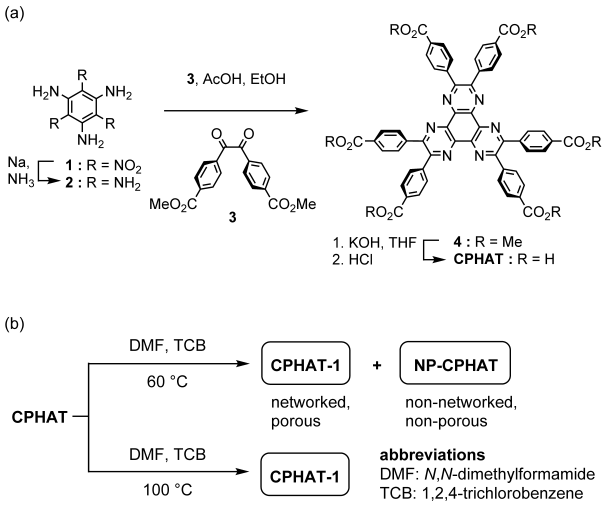

Scheme 1 (a) Synthesis and (b) crystallization conditions.

Table 1. Crystallographic parameters of **CPHAT-1-(TCB)**, **CPHAT-1a**, and **CPHAT-1-(I_2)**

crystal	**CPHAT-1-(TCB)**	**CPHAT-1a**	**CPHAT-1-(I_2)**
System	*Trigonal*	*Trigonal*	*Trigonal*
Space group	*P*-3	*R*-3	*R*-3
a, b / Å	37.2013(7)	37.1764(5)	37.1486(10)
c / Å	7.20124(15)	7.18907(10)	7.1441(4)
V / Å^3	8630.9(3)	8604.7(2)	8538.1(6)
R1	0.0574	0.0500	0.0608
wR2	0.1705	0.1504	0.1866
T / °C	−60	−60	−60
CCDC	1540571	1540572	1540570

low temperature such as at 60 °C, on the other hand, **CPHAT** yielded non-porous crystal **NP-CPHAT** as well as **CPHAT-1-(TCB)** concomitantly (Figure S1). In **NP-CPHAT**, one carboxylic group of CPHAT forms a H-bond with the nitrogen atom in the core, preventing formation of a porous networked framework (Table S1, Figure S2).

Crystallography

Crystal **CPHAT-1**, with the space group of *P*-3, exhibits a porous framework based on hexagonally arranged **CPHAT** molecules (Table 1 and Figure 2a). **CPHAT** molecule is one-dimensionally stacked in an AB pattern with the staggered twisting angle of 60°and intermolecular distances of 3.6 Å (Figure 2b). The resultant stacking columns are arranged in hexagonal manner,

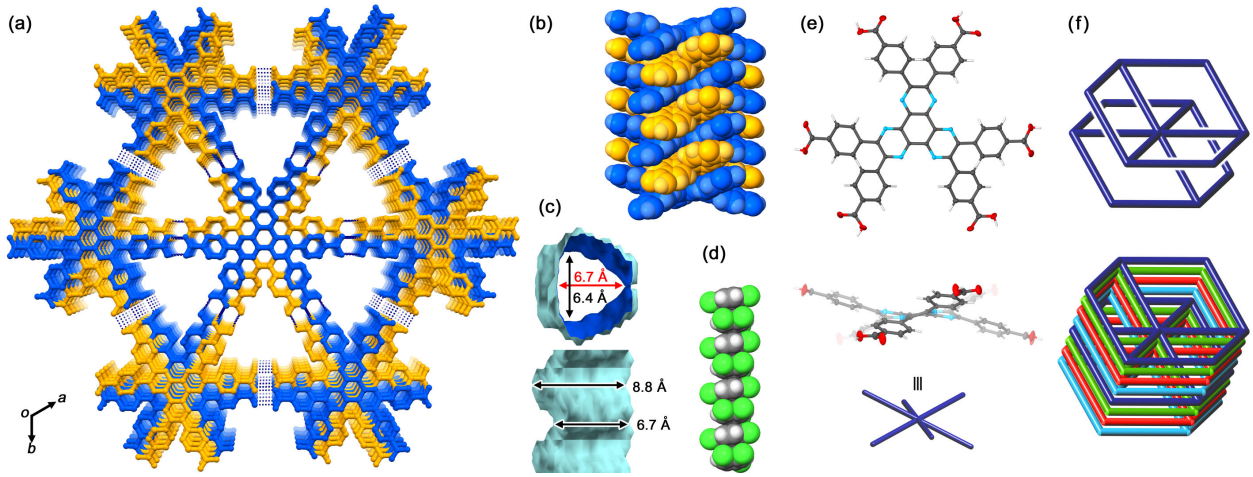

Figure 2. Crystal structure of **CPHAT-1-(TCB)**. (a) Packing diagram. (b) 1D Columnar structure composed of π-stacked **CPHAT** molecules. (c) Visualized surface of inclusion channels running along the *c* axis. (d) 1D structure of guest molecules (TCB) aligned in the inclusion channel. (e) Non-planar conformation of **CPHAT** drawn in anisotropic displacement ellipsoids with 50% probability. (f) Schematic representations of (top) single and (bottom) 4-fold inter-penetrated H-bonded frameworks with ***pcu*** (primitive cubic) topology (point symbol of the net: $[4^{12}.6^3]$).

allowing formation of 1D inclusion channels along the *c* axis. The channel has a triangular shaped cross section with the width ranging 6.7 to 8.8 Å and ratio of solvent accessible volume per the unit cell is 31% (Figure 2c). Molecules of TCB are accommodated in the channel in a parallel fashion with a host/guest ratio of 1/2 (Figure 2d).

It is noteworthy that **CPHAT** molecule is not flat but has a twisted conformation: Root mean square deviation (RMSD) of the twisted HAT core from the mean square plane is 0.196 Å, which is larger by 0.106 Å than that in the previously reported 2D networked system **Tp-1**.[8] The six peripheral carboxyphenyl groups in **CPHAT** alternately direct up and down with an angle of ca. 30° against the central benzene ring of HAT core (Figure 2e). Dihedral angle between the peripheral phenylene groups and HAT core, on the other hand, is much smaller compared with those in **Tp-1** systems[8b] because of lack of sterical hindrance caused by hydrogen atoms at the *ortho*-positions: the dihedral angle in the present **CPHAT-1-(TCB)** and previous **Tp-1** systems are 25.5–28.0° and 54.7–76.1°,[8b] respectively. These structural features of **CPHAT** and **Tp** are also consistent with those of optimized structures calculated at the B3LYP/6-31G* level, although molecular geometries in crystalline states are strongly affected by packing force (Figure S4).

The observed structural features of **CPHAT** made it possible to form a three-dimensionally extended H-bonded framework. In contrast to a H-bonded motif with a planar cyclic shape in **Tp** systems, **CPHAT** molecules are networked via an infinite three-fold helical motif with a helical pitch of 14.4 Å (Figure 1b). Consequently, **CPHAT** forms a three-dimensionally-networked framework expressed by ***pcu*** (primitive cubic) 4^6-net of network topology (point symbol of the net: $[4^{12}.6^3]$) (Figure 2f).[14,15] The network is interpenetrated by 4-fold to give rigid porous structure. It is interesting that C_3-symmetric planar molecule yields a framework with the network topology as same as that of a cubic framework such as MOF-5 (Figure S3).[16]

Thermal behavior of CPHAT-1-(TCB).

To obtain the information about activation condition, crystalline bulk of **CPHAT-1-(TCB)** was subjected to thermogravimetric (TG) analysis as shown in Figure 3a. The TG curve exhibits gradual weight loss of 28% up to ca. 300 °C, indicating that TCB molecules were almost all removed at around this temperature although the solvent molecules are not easily removed due to a narrow inclusion channel well-fitted to the solvent molecules. Further weight loss at temperature higher that ca. 350 °C is caused by thermal decomposition of **CPHAT**. An endothermic behavior in the differential thermal analysis (DTA) curve at 350 °C to 365 °C also supports the thermal decomposition (Figure S6).

To obtain structural information during desolvation by heating, PXRD patterns were recorded as heating as-formed crystalline bulk of **CPHAT-1-(TCB)** (Figure 3b). The intensity of the diffraction peaks at 4.7°, 8.2°, 9.5°, and so on increases due to release of TCB until temperature reached to 200 °C. The peak positions of the diffraction are the same as those of as-formed crystalline bulk of **CPHAT-1-(TCB)**, indicating that no structural change occurred upon desolvation. The diffraction peaks started to decay from 339 °C and simultaneously new weak peaks generated at 8.7°, 10.2°, 13.3°, 15.8°, and so on, indicating that original structure collapsed and changed into another one.

Stability of CPHAT-1a.

On the basis of the above described thermal behaviors, desolvation of **CPHAT-1-(TCB)** was accomplished at 200 °C under vacuum condition for 48 h to yield the activated crystalline

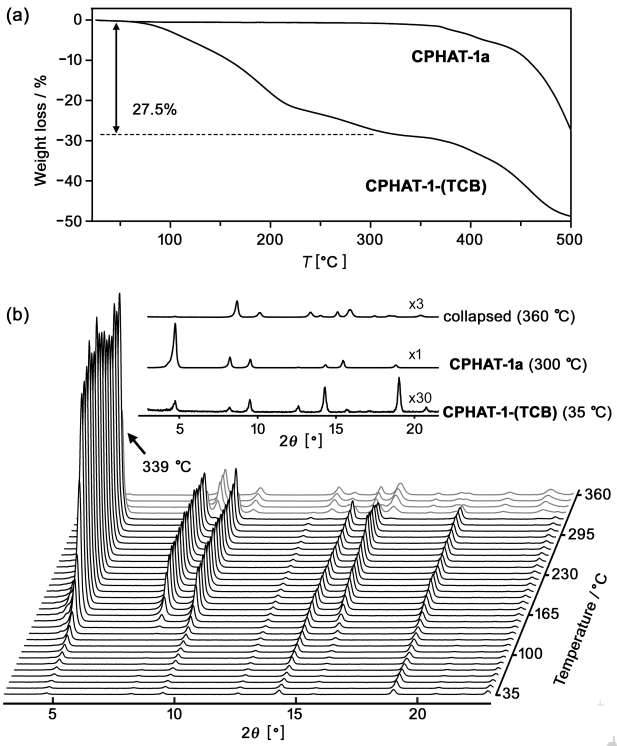

Figure 3. Thermal behaviors of **CPHAT-1-(TCB)** and its activated form **CPHAT-1a**. (a) Thermogravimetric (TG) analysis of as-formed **CPHAT-1-(TCB)** and activated **CPHAT-1a** crystalline bulks. Weight loss of 28% at ca. 300 °C is corresponding to the theoretical value calculated on the basis of the crystallographically-determined host:guest ratio of 1:2. (b) Changes of powder X-ray diffraction (PXRD) patterns of as-formed **CPHAT-1-(TCB)** upon desolvation by heating. The pattern of **CPHAT-1a** starts to collapse at ca. 339 °C. Inset: Representative PXRD patterns of as-formed **CPHAT-1-(TCB)** (bottom), desolvated **CPHAT-1a** (middle), and the collapsed form (top).

material **CPHAT-1a**. Removal of TCB was confirmed by ^{1}H NMR spectrum of the resulting material dissolved in a DMSO-d_6 solution (Figure S7). TG curve of **CPHAT-1a** also supported the desolvation: weight loss of ca. 1% was observed before rapid weight loss at 355 °C due to decomposition of the compound (Figure 3a).

As shown in Figure 4a, crystalline bulk of **CPHAT-1a** shows uniformed birefringence features in polarized optical microscope (POM) images. Scanning electron microscope (SEM) images also show that **CPHAT-1a** retains a clear crystalline habit of a hexagon rod with diameter up to 10 μm (Figures 4b and S8). These results strongly indicate that **CPHAT-1a** retains not only the PXRD profile but single-crystallinity after activation due to robust three dimensional networking. Remarkably, we succeeded in crystallographic analysis on single crystals of **CPHAT-1a**, revealing that **CPHAT-1a** has the same framework as **CPHAT-1-(TCB)** (Table 1), thought the channel is empty. **CPHAT-1a** belongs to the space group *R*-3, which is different from that of **CPHAT-1** (*P*-3) due to the existence of low symmetric guest molecule (*i.e.*, TCB) in the void space.

Furthermore, we revealed that the framework of **CPHAT-1a** resisted both water and acidic conditions. As shown in Figure 5,

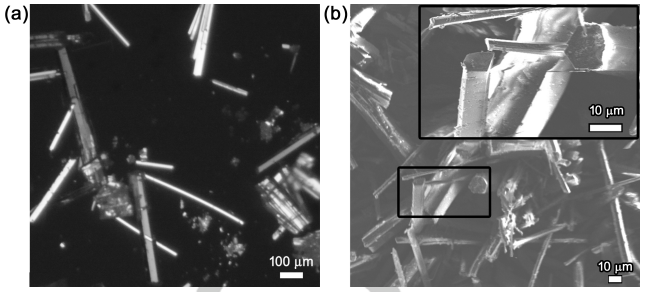

Figure 4. (a) POM and (b) SEM images of **CPHAT-1a** crystal-line bulk. (Inset: magnified SEM image)

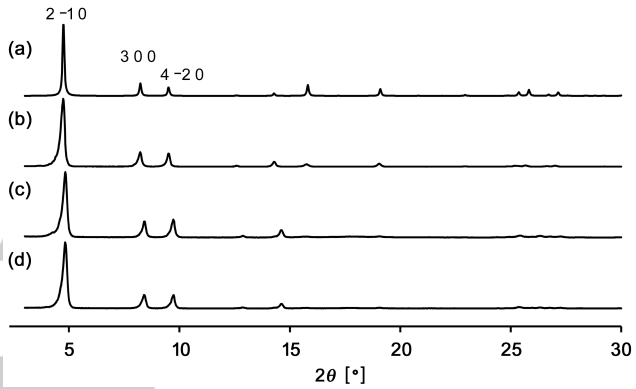

Figure 5. PXRD patterns of crystalline bulk of **CPHAT-1a**. (a) Simulated pattern from the crystallographic data. (b) Experimental pattern before soaking. (c) Pattern after ex-posing water at 60 °C for 24 h. (d) Pattern after exposing 10%-HCl aqueous solution at 60 °C for 24 h.

PXRD patterns of crystalline bulk of **CPHAT-1a** retain the original profile after soaking in hot water at 60 °C for 24 h and in 10%-HCl aqueous solution at 60 °C for 24 h, although **CPHAT-1a** was immediately dissolved in basic aqueous solution such as KOH aqueous solution.

Sorption experiments of gases and iodine.

The permanent porosity of **CPHAT-1a** was evaluated by nitrogen, hydrogen, and carbon dioxide molecules sorption experiments at low temperature (77 K, 77 K, and 195 K, respectively) as shown in Figure 6a. **CPHAT-1a** exhibits almost no adsorption of N_2 and H_2: Uptakes are 7.1 $cm^3 g^{-1}$ (0.32 mmol g^{-1}) and 2.6 $cm^3 g^{-1}$ (0.12 $mmolg^{-1}$), respectively, at relative pressure (p/p_0) of 0.99. N_2 adsorption was also conducted at 195 K to confirm a low temperature effect,[17] resulting in a increase of uptake (21 $cm^3 g^{-1}$, 0.95 $mmolg^{-1}$). For carbon dioxide, on the other hand, **CPHAT-1a** show an uptake of 137 $cm^3 g^{-1}$ (6.13 mmol g^{-1}) at p/p_0 of 0.99 with a typical type-I isotherm. Calculated BET surface area based on the isotherm of carbon dioxide is 649 $m^2 g^{-1}$. The gas sorption behavior of **CPHAT-1a** is different from that of analogous system, such as **Tp-apo**, possessing 1D channels composed of H-bonded PhT motifs previously we reported.[8c] Namely, **Tp-apo** shows

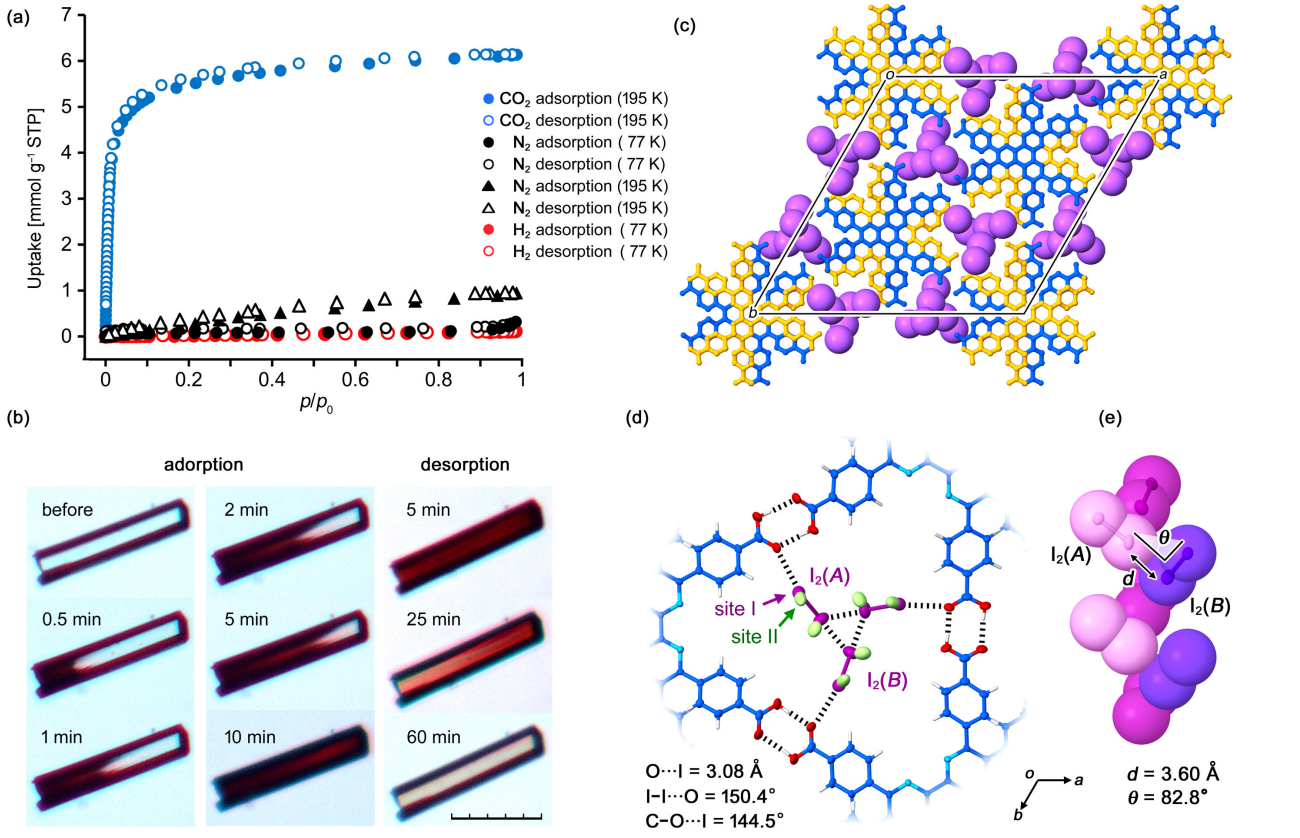

Figure 6. Sorption properties of **CPHAT-1a**. (a) Gas sorption isotherms. CO_2: light blue, N_2: black, H_2: red. Solid symbol: absorption process, open symbol: desorption process. (b) Photographs for Iodine sorption and desorption of single crystal of **CPHAT-1a**. Scale bar: 100 μm. (c) Crystal structure of **CPHAT-1-(I_2)**, in which iodine is drawn by space-fill model. Color code, **CPHAT**: yellow or blue, I_2: purple. (d) Interactions among the carboxyl groups and iodine molecules in **CPHAT-1-(I_2)**. Iodine molecules are disordered into two sites (I and II) with an abundance ratio of 0.61 and 0.39, respectively, although for clarity, only the major population is shown in (c). The occupancy of total iodine molecules in the channel is 79%. (e) Three-fold helical alignment of iodine molecules in the site I. *d* and θ the intermolecular distance and contact angle between the neighbouring iodine molecules, respectively. Symmetry cords: (A) x, y, y; (B) −1/3−x+y, 1+1/3−x, 1/3+z.

equal amounts of uptake toward both carbon dioxide and nitrogen molecules, while **CPHAT-1a** shows selective absorption for the former. CO_2 adsorption selectivity over N_2 has been explained by three aspects: (1) smaller kinetic diameter of CO_2,[18] (2) more attractive and stronger interaction of the gas molecules with pore surfaces due to a large quadrupole moment (enthalpy factor),[19] and (3) N_2-phobic nature of the framework (entropy factor).[20] In the present systems, the width of the channels (~6.7Å) is larger than the kinetic diameters of nitrogen (3.6 Å) and carbon dioxide molecules (3.3 Å). However, the slightly wider channel of **Tp-apo** (by 1.5 Å) compared to that of **CPHAT-1a** (Figure S9), can have significant effect on the sorption behavior in connection with factors (2) and (3).

To achieve one-dimensionally aligned supramolecular structure of iodine molecules,[21] we attempted to introduce iodine into the channel of **CPHAT-1a**. Crystals of **CPHAT-1a** were exposed to iodine vapor at ambient condition, resulting in penetration of iodine into the crystals. As shown in Figure 6b, an edge of a single crystal of **CPHAT-1a** was immediately colored with dark red, and the colored region was extended and reached to the other edge within 10 min, giving iodine included crystal **CPHAT-1-(I_2)**. The rate of iodine penetration depends on sizes, shapes, and conditions (e.g. existence of cracks) of the selected single crystals. After removing the iodine source, the colored crystals were then gradually discolored from the edge that colored first in the absorption process in relatively longer period of time compared with the absorption process (*e.g.* 60 min for the present system, Figure 6b).

To identify an iodine-included structure and interaction among iodine molecules and **CPHAT** molecular units in the crystal, **CPHAT-1-(I_2)** was subjected to single-crystal X-ray diffraction analysis at −60 °C. As a result, we revealed that **CPHAT-1-(I_2)** has the same framework and the nearly identical cell parameters with **CPHAT-1a** (Table 1), and moreover, that iodine molecules are accommodated in the channels (Figure 6c). The iodine in the channel is disordered into two positions (sites I and II) with an abundance ratio of 0.61 and 0.39 (Figure 6d). The occupancy of total iodine molecules was estimated by crystallographic analysis to be 79%, indicating strong affinity between iodine and surface of the channel. Indeed, the iodine

molecule form a halogen-bond[22] with the oxygen atom of the carboxy group on the channel surface [distance of O···I: 3.08 Å, angles of I–I···O and C–O···I: 150.4° and 144.5°, respectively]. In the channel, iodine molecules are aligned in a three-fold helical fashion (Figure 6e). Each of iodine molecules contacts with the neighboring ones with a nearly perpendicular manner [e.g. I_2(A) and I_2(B)]: the intermolecular distance (*d*) and contact angle between the neighboring iodine molecules (θ) are 3.60 Å and 82.8°, respectively, which are typical values for the perpendicular halogen-bond in a crystalline state.[23]

Steady-state photobehavior

We carried out UV-vis absorption and emission measurements of **CPHAT** and its methyl ester derivate **4** in DMF where both chromophores are relatively well soluble (Figure S10). The UV-vis absorption spectra present similar shape with a maximum at 368 and 359 nm for **CPHAT** and **4** respectively. Previous studies of the parent molecule, HAT, have shown that the UV-vis absorption spectrum in chloroform presents a maximum at 260 nm corresponding to the S0→S3 transitions, along with a broad unresolved band around 300 nm, assigned to the S0→S2 transition.[24] HAT structure presents a D_{3h} symmetry, making forbidden the S0→S1 transition. A theoretical study suggests that the forbidden transition should be located around 350 nm. Our data show that the absorption spectra of both **CPHAT** and **4** in DMF are characterized by strong absorptions at 368 and 359 nm, respectively. We assign them to S0→S1 transition, reflecting a change in the symmetry of this chromophore when compared with the parent HAT. This change is clearly associated with the presence of the benzoic acid substituents around the core, in agreement with our theoretical calculations (Figure S5). As mentioned above, **CPHAT** molecule has a twisted conformation and the RMSD of the twisted HAT core from the mean square plane is 0.196 Å. Additionally, the absorption spectra of **CPHAT** and **4** show a red-shift compared to that of HAT, and which can be ascribed to a larger π-conjugation, owing to the phenyls and carboxylic groups. Other systems have shown similar red shift in the absorption spectra as a result of increase in the electron density.[25]

The emission spectra of **CPHAT** and **4** in DMF have a maximum intensity at 444 and 419 nm, respectively. The abnormal Stockes shift values (4650 and 4000 cm^{-1} for **CPHAT** and **4**, respectively) are results of an intramolecular charge transfer (ICT) reaction at the S1 state. The full-width at half-maximum (FWHM) of the emission band of **CPHAT** (3650 cm^{-1}) is significant larger than that of **4** (3000 cm^{-1}), and reflects the formation of another excited species in **CPHAT**. Indeed, its emission band shows a long tail at the red side of the spectrum (Figure S10). The fluorescence quantum yields (φ) of **CPHAT** and 4 (0.04 and 0.05, respectively) are low due to an efficient crossing from (π-π*) to no fluorescent (n-π*) states, caused by the presence of nitrogen atoms. Next part will give us information on the excited state relaxation.

Time-resolved photobehavior

To get information on the photodynamics of **CPHAT** and **4** in DMF solutions, we performed picosecond time-resolved studies, exciting at 370 nm and observing at different wavelengths. Figures 7a and S11a show representative emission decays of **CPHAT** and **4** in DMF solutions, respectively. Also, Table S2 gives the time constants (τi), contributions (ci) and preexponential factors (ai normalised to 100) obtained from multiexponential global fits of the decays. For **4**, we got two decaying components, whose times are 160±30 ps and 2.41±0.20 ns. The contribution of the shorter decay is larger than that of the longer one. Based on solvent effect on emission spectra of molecular systems that present the same core (HAT) with different surrounding structures, an ICT process has been suggested to occur.[26] Our time-resolved results point out to an ICT process within **4** in DMF, whose time is < 15 ps (the time resolution of our picosecond setup). Thus, we assign the shortest component, 160±30 ps, to the lifetime of the initially excited species, and which photoproduces a charge transfer structure, whose emission lifetime is 2.41±0.20 ns (Figure S11c). The fluorescence decays of **CPHAT** in DMF exhibit a complex multiexponential behaviour, with time constants of 70±20 ps, 0.23±0.05, 1.0±0.1 and 4.90±0.20 ns (Table S2). The shortest component is decaying at the bluest part of the spectrum, and becomes a rising one from 525 nm. The intermediate times, 0.23±0.05 and 1.0±0.1 ns, are decaying in all the spectral range. Finally, the longest component (4.90±0.20 ns) does not appear at the blue part of the spectrum and decays from 500 nm. To explain this complex and rich behaviour, we suggest the involvement of two processes at the S1 state, and explained it by following (Figure 7c). Upon electronic excitation of **CPHAT**, a fast ICT takes places (<15 ps), as it occurs in **4**. The initially excited **CPHAT** has a fluorescence lifetime of 230±50 ps, while the photoproduced ICT species decays in 1 ns. Moreover, as a result of ICT where a large electronic redistribution has occurred, the ICT structure of **CPHAT** becomes more acidic as it has a carboxylic group, and undergoes an intermolecular excited-state proton-transfer (PT) reaction to the surrounding solvent (DMF), which has a high basicity through its H-bonding ability (β=0.69).[27] Our analysis of the fluorescence decays at different wavelengths of observation shows that this time is 70±20 ps. Previous study of comparable HOF systems showed the formation of this kind of H-bonds in DMF, and which play a key role in the crystals formation, morphology and stability.[8] Finally, the resulting formed anion species of **CPHAT** has an emission lifetime of 4.90±0.20 ns (Figure 7c).

To get more information on the spectral photodynamics of **CPHAT** and **4** in DMF solutions, we recorded the time-resolved-emission spectra (TRES), following excitation at 370 nm (Figures 7b and S11b, respectively). The TRES of **4** at early times (<1 ns) are characterized by an emission band centred on 425 nm that decreases in intensity as time increases. This behaviour is concomitant with the appearance at longer times of a new band with a maximum of emission intensity at 475 nm, and which is reminiscent to the presence of a photoproduced charge transfer species. Note that this band is not clear in the CW emission spectrum, as its intensity is weaker than the one at 425 nm. Figure 7b shows the TRES of CPHAT in DMF. At t = 0 ps, the early band which appears at 435 nm is assigned to the emission of the

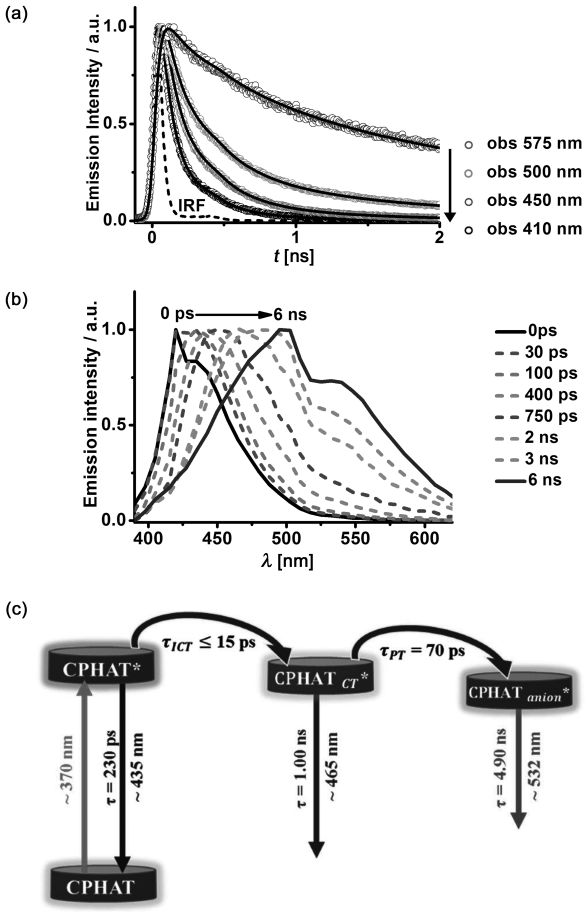

Figure 7. (a) Emission decays of **CPHAT** in DMF upon excitation at 390 nm, and observation at the indicated wavelengths. The solid lines are from the best-fit using a multiexponential function. (b) Normalized time-resolved emission-spectra of **CPHAT** in DMF upon excitation at 370 nm, and gating at the indicated delay times. The peak at 420 nm is from the solvent raman emission. (c) Proposed photodynamic scheme for **CPHAT** in DMF solutions, where τ_{ICT} and τ_{PT} are the times for intramolecular charge transfer and intermolecular proton transfer reactions.

initially excited **CPHAT** population. The peak at 420 nm arises from the Raman signal of the solvent. As the gating time increases, the spectrum shifts to longer wavelengths, and becomes wider. The spectral shift from 0 to 6 ns gating time is large; about 3070 cm^{-1}. This confirms the photoproduction of another structure (ICT one) from the initially excited species. At gating times longer than ~750 ps, the spectrum exhibits a new band whose maximum is centred at 532 nm, and a red shift of 4200 cm^{-1}. This time-dependent spectral photobehavior indicates a subsequent process within the ICT structure. Thus, while the earliest spectral shift reflects the ICT process within the initially excited species, the latest one is due to a subsequent CPHAT anion formation as explained above (Figure 7c).

Solid-state Photobehaviour

It is natural to think that **CPHAT-1-(TCB)** and **CPHAT-1a** crystals may show photoinduced charge-carrier transport ability owing to the 1D stacked rigid structure of **CPHAT**. Therefore, their crystalline bulks were subjected to flash-photolysis time-resolved microwave (FP-TRMC) measurements.[28] Surprising, neither crystalline bulks of these crystals show charge transport ability. The observed insulation property is presumably brought from the fact that **CPHAT** moieties are stacked with 60° rotation, which is known as the unfavourable arrangements for efficient hopping of charge carrier species.[29] **CPHAT-1-(TCB)** and **CPHAT-1a** crystal bulks show fluorescence bands with emission maxima at 460 nm, and the quantum efficiencies are 0.041 and 0.016, respectively. These low values reflect efficient crossing from (π, π*) state to the less emissive (n, π*) one, as happening in solutions. It should be noted that other no-radiative decay channels might be accessible in solid state, as a result of stacking molecular interactions.[30] Finally, crystals of **CPHAT** trapping iodine molecules, **CPHAT-1(I_2)**, have a complete emission quenching due to a charge transfer between the chromophore of the crystals and iodine molecules, in agreement with the X-ray diffraction results (Figure 6d). The following paragraph will provide us information on the fluorescence at a single crystal level.

Single Crystal Fluorescence Microscopy

To get precise information of solid state fluorescence, we conducted fluorescence confocal microscopy measurements on single crystals of **CPHAT-1-(TCB)** and **CPHAT-1a**. The emission spectra of **CPHAT-1-(TCB**) and **CPHAT-1a** have emission maxima at 458 nm and 450 nm, respectively (Figure 8a). Additionally, **CPHAT-1-(TCB)** has a broad shoulder at around 550 nm, which is not observed in that of **CPHAT-1a**. The emission decays, recorded over the entire emission spectrum of **CPHAT-1a**, give lifetimes of τ_1 = 0.20 ± 0.05 ns (92%) and τ_2 = 0.8± 0.1 ns (8%), while those of **CPHAT-1-(TCB)** are τ_1 = 0.30 ± 0.05 ns (85%), τ_2 = 1.40 ± 0.15 ns (12%), and τ_3 = 4.5 ± 0.2 ns (3%) (Figure 8b). However, when the decays were collected at blue (420 - 470 nm) and green (515 – 565 nm) part of the spectrum, the fits give: τ_1 = 0.30 ± 0.05 ns (90%) and τ_2 = 1.1± 0.1 ns (10%); and τ_1 = 0.90 ± 0.1 ns (85%) and τ_2 = 4.0± 0.1 ns (15%), respectively. The lifetimes at the blue emission are comparable to those of **CPHAT-1a**, suggesting that the emitters from both crystals in this spectral region are very similar in nature. On the other hand, the appearance of the red-edge shoulder in the emission spectrum of **CPHAT-1-(TCB)**, and the presence of the new, longer lifetime in the green spectral region indicate the action of specific interactions (H-bonds) between the carboxylic groups of the crystal building unit and those of TCB, in agreement with the results obtained for the **CPHAT** chromophore in DMF solutions. Within the experimental error, we observed no significant dependence of either the emission spectra position/shape or the emission lifetime values on the crystal orientation and the targeted position in the crystal. **4** under the microscope shows an emission band with a maximum at 455 nm, and a fluorescence lifetime of 0.31±0.05 (97%) and 1.80±0.20 (3%), similar to the obtained for **CPHAT-1a**. As **4** exhibits an amorphous structure, its fluorescence anisotropy is ~0 (Figure

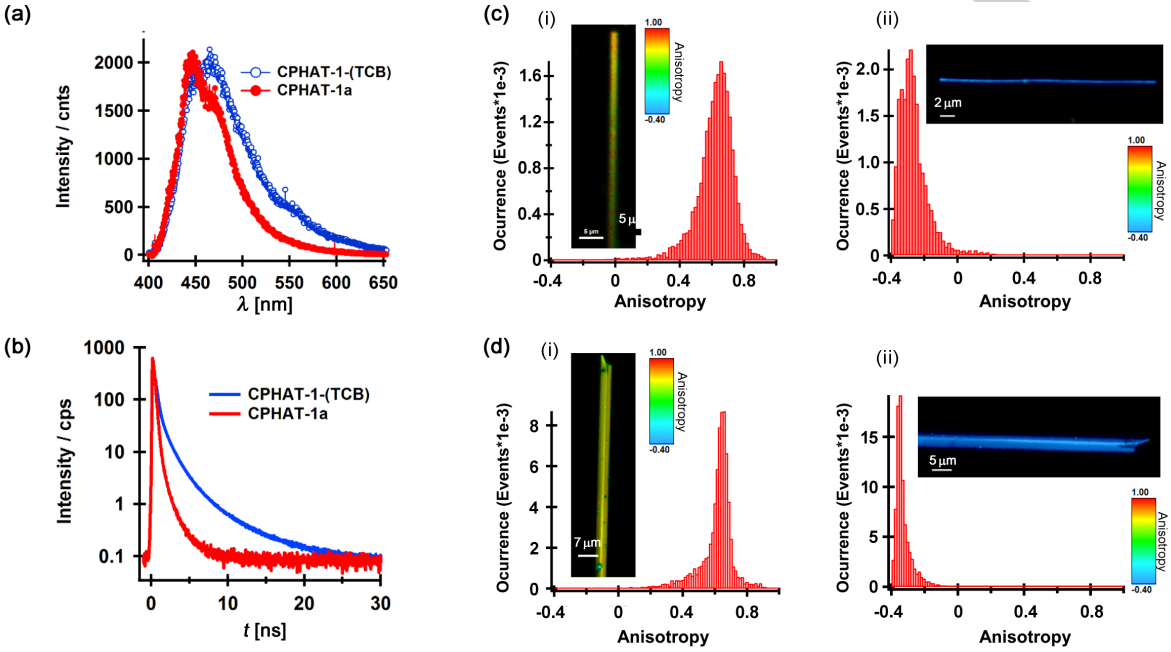

Figure 8. (a) Emission spectra and (b) decays of **CPHAT-1-(TCB)** (blue) and **CPHAT-1a** (red) single crystals. The excitation wavelength was 390 nm and the decays were measured over the whole spectral range using a 430 nm long-pass filter (HQ430LP, Chroma). Dependence of the emission anisotropy on the orientation of single crystals of (c) **CPHAT-1-(TCB)** and (d) **CPHAT-1a** with respect to the plane of observation. i) Histogram of the emission anisotropy for the horizontal crystal orientation; ii) histogram of the emission anisotropy for the vertical crystal orientation. (Insets) anisotropy distribution image for the corresponding crystal orientation. The anisotropy was calculated with respect to the excitation polarization (vertical). The limits for the anisotropy are -0.4 to 1.0, where -0.4 corresponds to perpendicular orientation and 1.0 to parallel.

S13). Remarkably, the single crystals of **CPHAT-1-(TCB)** and **CPHAT-1a** show highly anisotropic emission behaviours (Figure 8c,d). Both **CPHAT-1-(TCB)** and **CPHAT-1a** present similar values of the anisotropy that depend on the orientation of the crystals. The anisotropy for those oriented perpendicularly to the plane of observation has a value of 0.65, while those with parallel orientation give a value of -0.32. This behaviour (strong and in-sign different anisotropies) suggests an ordered crystalline structure for both **CPHAT-1-(TCB)** and **CPHAT-1a** with preferential orientation of the molecular dipole moments perpendicular to the long crystal axis. The emission polarization/anisotropy behaviour of the ordered parent molecules in the single crystals imply that they form a π-stack with the π-π stacking direction parallel to the length axis of the crystal. This observation is reminiscent to the crystal morphology and structure shown in Figure 2. Similar behaviour has been reported for other single crystalline molecular structures formed either by π-π stacking or J-aggregates interactions between the constituents [30c,31] It is remarkable that the anisotropy distribution histogram for **CPHAT-1-(TCB)** monocrystal is significantly broader (full width at half maximum, FWHM ~ 0.12) than the **CPHAT-1a** narrow one (FWHM ~ 0.05) (Figure 8a,b). This indicates that the presence of TCB molecules in the crystal structure of **CPHAT-1a** disrupts the π-π packing of the parent HAT molecules and leads to a more heterogeneous distribution of the molecular interactions between the chromophore building units within the studied **CPHAT-1-(TCB)** single crystals. We reflected this difference in the colour of the imaged crystals under different orientations (Figure 8c). On the contrary, the **CPHAT-1a** crystal exhibits a very homogenous distribution, as a result of similar interactions of the unit forming the crystal (Figure 8d). Thus, the observed difference in the FWHMs of the anisotropy distributions can act as a "ruler" of the molecular orientation within the crystal, which should be relevant to the defect formation, of great relevance for MOFs, COFs, and HOFs stability and use.[32]

Conclusion

We revealed that a new hexaazatriphenylene derivative with six carboxyphenyl groups, **CPHAT**, forms three dimensionally networked framework with pcu topology, which subsequently interpenetrated by 4-fold to yield porous HOF **CPHAT-1**. The activated **CPHAT-1a** retains not only permanent porosity but single-crystallinity. Furthermore, **CPHAT-1a** keeps its framework up to 340 °C, or in hot water, and in acidic aqueous solutions. Such structural stability of **CPHAT-1a** enables precise structural characterization of the framework accommodating guest molecules based on single crystalline X-ray diffraction analysis and evaluation of their structure dependent properties. These

results clearly show that even a simple H-bonding motif can be applied for construction of robust HOFs.

Surprisingly, **CPHAT** in DMF solutions exhibits a strong allowed S0→S1 transition, while it is prohibited in its parent molecule (the core), which does not display this absorption band. The change in the symmetry of **CPHAT** is due to the introduction of the benzoic groups in the core. These groups act as a glue to build up single crystals (of micrometers in length) having a clean rod shape. **CPHAT** molecule shows broad emission band as a result of an ultrafast ICT process followed by an intermolecular proton transfer reaction (70 ps) at the excited state with DMF molecules to generate the anion of **CPHAT**. Fluorescence microscopy study at single crystal level reveals an ordered crystalline structure for both **CPHAT-1-(TCB)** and **CPHAT-1a** with preferential orientation of the molecular dipole moments. Interestingly, the interaction of **CPHAT-1a** with TCB molecules in the formed crystal leads to a heterogeneous distribution of the molecular interactions as a result of H-bonds formation with the co-solvent upon crystal formation.

Acknowledgements

This work is supported by a Grant-in-Aid for Scientific Research (C) (JPT15K04591) and for Scientific Research on Innovative Areas: π-System Figuration (JP15H00998) from MEXT Japan, and by the MINECO and JCCM through projects: MAT2014-57646-P and PEII-2014-003-P. E.G. thanks the MEC (Spain) for the FPU fellowship. We thank Prof. Shu Seki at Kyoto University for FP-TRMC experiments and SEM measurements. Crystallographic data were partly collected using synchrotron radiation at the BL38B1 in the SPring-8 with approval of JASRI (proposal nos. 2015B1397, 2016A1121, and 2016B1151).

Keywords: porous organic framework • hydrogen bonds • carboxylic acid• crystal engineering• fluorescence

[1] (a) J. R. Holst, A. Trewin, A. I. Cooper, *Nat. Chem.* **2010**, *2*, 915-920; (b) X. Feng, X. Ding, D. Jiang, *Chem. Soc. Rev.* **2012**, *41*, 6010-6022; (c) M. Mastalerz, *Chem. Eur. J.* **2012**, *18*, 10082-10091; (d) S.-Y. Ding, W. Wang, *Chem. Soc. Rev.* **2013**, *42*, 548-568; (e) M. Dogru, T. Bein, *Chem. Commun.* **2014**, *50*, 5531-5546; (f) A. G. Skater, A. I. Cooper, *Science*, **2015**, *348*, 988; (g) P. J. Waller, F. Gándara, O. M. Yaghi, *Acc. Chem. Res.* **2015**, *48*, 3053-3063; (h) N. Huang, P. Wang, D. Jiang, *Nat. Rev. Mater.* **2016**, *1*, 16068.

[2] G. R. Desiraju, *Angew. Chem., Int. Ed. Engl.* **1995**, *34*, 2311-2327.

[3] Review for HOFs, see; J. Lu, R. Cao, *Angew. Chem.* **2016**, *128*, 9624-9630; *Angew. Chem. Int. Ed.* **2016**, *55*, 9474-9480.

[4] Examples of HOFs with permanent porosity, see; (a) A. R. A. Palmans, J. A. J. M. Vekemans, H. Kooijman, A. L. Spek, E. W. Meijer, *Chem. Commun.* **1997**, 2247-2248; (b) P. Sozani, S. Bracco, A. Comotti, L. Ferretti, R. Simonutti, *Angew. Chem.* **2005**, *117*, 1850-1854; *Angew. Chem. Int. Ed.* **2005**, *44*, 1816-1820; (c) Y. He, S. Xiang, B. Chen, *J. Am. Chem. Soc.* **2011**, *133*, 14570-14573; (d) M. Mastalerz, I. M. Oppel, *Angew. Chem.* **2012**, *124*, 5345-5348; *Angew. Chem. Int. Ed.* **2012**, *51*, 5252-5255; (e) X.-Z. Luo, X.-J. Jia, J.-H. Deng, J.-L. Zhong, H.-J. Liu, K.-J. Wang, D.-C. Zhong, *J. Am. Chem. Soc.* **2013**, *135*, 11684-11687; (f) T.-H.Chen, I. Popov, W. Kaveevivitchai, Y.-C.Chuang, Y.-S. Chen, O. Daugulis, A. J. Jacobson, O. Š. Miljanić, *Nat. Commun.* **2014**, *5*. 5131; (g) J. Lü, C. Perez-Krap, M. Suyetin, N. H. Alsmail, Y. Yan, S. Yang, W. Lewis, E. Bichoutskaia, C. C. Tang, A. J. Blake, R. Cao, M. Schröder, *J. Am. Chem. Soc.* **2014**, *136*, 12828-12831; (h) P. Li, Y. He, Y. Zhao, L. Weng, H. Wang,R. Krishna, H. Wu, W. Zhou, M. O'Keeffe, Y. Han, B. Chen, *Angew. Chem.* **2015**, *127*, 584-587; *Angew. Chem. Int. Ed.* **2015**, *54*, 574-577. (i) H. Wang, B. Li, H. Wu, T.-L. Hu, Z. Yao, W. Zhou, S. Xiang, B. Chen. *J. Am. Chem. Soc.* **2015**, *137*, 9963-9970.

[5] O. Ivasenko, D. F. Perepichka, *Chem. Soc. Rev.* **2011**, *40*, 191-206.

[6] (a) D. J. Duchamp, R. Marsh, *Acta. Crystallogra. B* **1969**, *25*, 5–19; (b) F. H. Herbstein, M. Kapon, G. M. Reisner, *J. Inclusion Phenom.* **1987**, *5*, 211–214; (c) K. Kobayashi, T. Shirasaka, E. Horn, N. Furukawa, *Tetrahedron Lett.* **2000**, *41*, 89–93; (d) I. Hisaki, N. Q. E. Affendy, N. Tohnai, *CrystEngComm* **2017**, in press.

[7] (a) C. A. Zentner, H. W. H. Lai, J. T. Greenfield, R. A. Wiscons, M. Zeller, C. F. Campana, O. Talu, S. A. FitzGerald, J. L. C. Rowsell, *Chem. Commun.* **2015**, *51*, 11642-11645; (b) S. Nandi, D. Chakraborty, R. Vaidhyanathan, *Chem. Commun.* **2016**, *52*, 7249-7252; (c) F. Hu, C. Liu, M. Wu, J. Pang, F. Jiang, D. Yuan, M. Hong, *Angew. Chem.* **2017**, *129*, 2133-2136; *Angew. Chem. Int. Ed.* **2017**, *56*, 2101-2104.

[8] (a) I. Hisaki, S. Nakagawa, N. Tohnai, M. Miyata, *Angew. Chem.* **2015**, *127*, 3051-3055; *Angew. Chem. Int. Ed.* **2015**, *54*, 3008-3012; (b) I. Hisaki, N. Ikenaka, N. Tohnai, M. Miyata, *Chem. Commun.* **2016**, *52*, 300-303. (c) I. Hisaki, S. Nakagawa, N. Ikenaka, Y. Imamura, M. Katouda, M. Tashiro, H. Tsuchida, T. Ogoshi, H. Sato, N. Tohnai, M. Miyata, *J. Am. Chem. Soc.* **2016**, *138*, 6617-6628; (d) I. Hisaki, S. Nakagawa, H. Sato, N. Tohnai, *Chem. Commun.* **2016**, *52*, 9781-9784.

[9] (a) J. L. Segura, R. Juárez, M. Ramos, C. Deoane, *Chem. Soc. Rev.* **2015**, *44*, 6850-6885.

[10] S. Kitagawa, S. Masaoka, *Coord. Chem. Rev.* **2003**, *246*, 73-88.

[11] M. Shatruk, A. Chouai, K. R. Dunbar, *Dalton Trans.* **2006**, 2184-2191. (b) J. R. Galán-Mascarós, K. R. Dunbar, *Chem. Commun.* **2001**, 217-218.

[12] S.-Q. Xu, T.-G. Zhan, Q. Wen, Z.-F. Pang, X. Zhao, *ACS Macro Lett.* **2016**, *5*, 99-102.

[13] D. Z. Rogers, *J. Org. Chem.* **1986**, *51*, 3904-3905.

[14] O. D. Friedrichs, M. O'Keeffe, O. M. Yaghi, *Acta Crystallogr. A* **2003** *59*, 22-27.

[15] ToposPro, the program package for multipurpose geometrical and topological analysis of crystal structures, was used for evaluation of the network topology, see; E. V. Alexandrov, V. A. Blatov, A. V. Kochetkov, D. M. Proserpio, *CrystEngComm* **2011**, *13*, 3947-3958.

[16] M. Li, M. O'Keeffe, O. M. Yaghi, *Chem. Rev.* **2014**, *114*, 1343-1370.

[17] T. K. Maji, R. Matsuda, S. Kitagawa, *Nat. mater.* 2007, 6, 142-148.

[18] M. R. Hudson, W. L. Queen, J. A. Mason, D. W. Fickel, R. F. Lobo, C. M. Brown, *J. Am. Chem. Soc.* **2012**, *134*, 1970-1973.

[19] J. Lü, C. Perez-Krap, M. Suyetin, N. H. Alsmail, Y. Yan, S. Yang, W. Lewis, E. Bichoutskaia, C. C. Tang, A. J. Blake, R. Cao, M. Schröder.

[20] H. A. Patel, S. H. Je, J. Park, D. P. Chen, Y. Jung, C. T. Yavuz, A. Coskun, *Nat. Commun.* **2013**, 4:1357.

[21] Examples for iodine sorption of porous materials, see; (a) T. Hasell, M. Schmidtmann, A. I. Cooper, *J. Am. Chem. Soc.* **2011**, *133*, 14920-14923; (b) J. Martí-Rujas, N. Islam, D. Hashizume, F. Izumi, M. Fujita, M. Kawano, M. *J. Am. Chem. Soc.* **2011**, *133*, 5853-5860. (c) Z. Yin, Q.-X. Wang, M.-H. Zeng, *J. Am. Chem. Soc.* **2012**, *134*, 4857-4863; (d) W.-Q. Xu, Y.-H. Li, H.-P. Wang, J.-J. Jiang, D. Fenske, C.-Y. Su, *Chem. Asian. J.* **2016**, *11*, 216-220; (e) S.-S. Zhao, L. Chen, X. Zheng, L. Wang, Z. Xie, *Chem. Asian J.* **2017**, *12*, 615-620.

[22] H. S. El-Sheshtawy, B. S. Bassil, K. I. Assaf, U. Kortz, W. M. Nau, *J. Am. Chem. Soc.* **2012**, *134*, 19935-19941.

[23] F. van Bolhuis, P. B. Koster, T. Migchelsen, *Acta Crystallogra.* **1967**, *23*, 90-91.

[24] R. Juárez, M. M. Oliva, M. Ramos, J. L. Segura, C. Alemán, F. Rodríguez-Ropero, D. Curcó, F. Montilla, V. Coropceanu, J. L. Brédas, Y. Qi, A. Kahn, M. C. Ruiz Delgado, J. Casado, J. T. López Navarrete, *Chem. Eur. J.* **2011**, *17*, 10312-10322.

[25] H. Nishide, M. Takahashi, J. Takashima, Y.-J. Pu, E. Tsuchida, *J. Org. Chem.* **1999**, *64*, 7375-7380.

[26] T. Ishi-i, Y. Moriyama, Y. Kusakaki, *RSC Adv*. **2016**, *6*, 86301-86308.

[27] M. J. Kamlet, J. L. M. Abboud, M. H. Abraham, R. W. Taft, *J. Org. Chem.* **1983**, *48*, 2877-2887.

[28] For review, see; (a) A. Saeki, Y. Koizumi, T. Aida, S. Seki, *Acc. Chem. Res.* **2012**, *45*, 1193–1202; (b) S. Seki, A. Saeki, T. Sakurai, D. Sakamaki, *Phys. Chem. Chem. Phys*. **2014**, *16*, 11093–11113.

[29] X. Feng, V. Marcon, W. Pisula, M. R. Hansen, J. Kirkpatrick, F. Grozema, D. Andrienko, K. Kremer, K. Müllen, *Nat. Mater.* **2009**, *9*, 421-426.

[30] (a) N. J. Hestand, F. C. Spano, *Acc. Chem. Res.* **2017**, *50*, 341-350; (b) Y. Liu, S. Ma, B. Xu, W. Tian, *Faraday Discuss*. **2017**, *196*, 219-229; (c) S. Qu, Q. Lu, S. Wu, L. Wang, X. Liu, *J. Mater. Chem*. **2012**, *22*, 24605–24609; (d) F. C. Spano, *Acc. Chem. Res*. **2010**, *43*, 429-439. (e) S. A. Jenekhe, J. A. Osaheni, *Science* **1994**, *265*, 765-768.

[31] (a) T. E. Kaiser, H. Wang, V. Stepanenko, F. Würthner, *Angew. Chem*. **2007**, *119*, 5637-5640; *Angew. Chem. Int. Ed*. **2007**, *46*, 5541 –5544; (b) X. Xiao, Z. Wang, Z. Hu, T. He, *J. Phys. Chem. B* **2010**, *114*, 7452–7460.

[32] M. D. Allendorf, C. A. Bauer, R. K. Bhakta, R. J. T. Houk, *Chem. Soc. Rev*. **2009**, *38*, 1330-1352.

Entry for the Table of Contents (Please choose one layout)

Layout 1:

FULL PAPER

Significantly robust hydrogen-bonded organic framework retaining permanent porosity and single-crystallinity was established with hexaazatriphenylene derivative (**CPHAT**), enabling precise structural characterization and property evaluations.

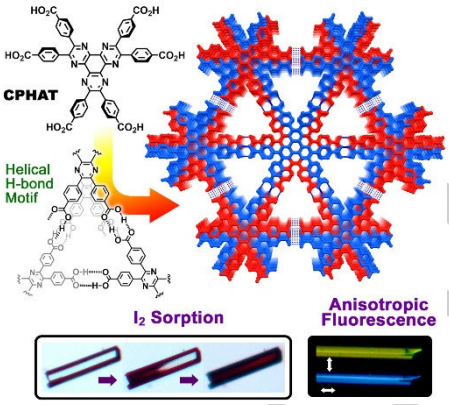

I. Hisaki, N. Ikenaka, E. Gomez, B. Cohen, N. Tohnai, A. Douhal**

Page No. – Page No.

Hexaazatriphenylene-Based, Hydrogen-Bonded Organic Framework with Permanent Porosity and Single-Crystallinity: Synthesis, Structural, Uptaking and Photophysical Characterization